An Investigation of the effect of Integrating Graphene Oxide on Sodium Yttrium Fluoride Gel on Its Electrochemical Performance as a Battery Electrode

Latifa Hamad Abdulla Hashem Alghafri

A Thesis

submitted in partial fulfillment of the

requirements for the degree of

Masters of Science

University of Washington

2024

Committee:

Peter Pauzauskie

Devin MacKenzie

Program Authorized to Offer Degree:

Material Science and Engineering

University of Washington

Abstract

An Investigation of the effect of Integrating Graphene Oxide into a Sodium Yttrium Fluoride Gel on Its Electrochemical Performance as a Battery Electrode

Latifa Alghafri

Supervisor: Associate Professor Peter J. Pauzauskie

Department of Material Science and Engineering

To cope with the rise in energy demands and climate crisis better batteries with higher energy densities are required. Lithium ion batteries (LIBs) are well established and studied but face issues of material abundance and cost. Fluoride ion batteries (FIBs) present an alternative but require more research into electrode, electrolyte and cell architecture. This study integrated Graphene Oxide into a Sodium Yttrium Fluoride (NaYF) gel through the addition to one of the precursor solutions. NaYF materials undergo multi step crystallization that develops materials with high surface areas and holds an affinity for ion replacement during synthesis making it an ideal candidate for electrochemical applications. XRD results confirmed the resulting gel was amorphous with a small degree of crystallinity and Graphite peaks. TEM confirmed the Graphene Oxide's incorporation within the gel's pores. BET analysis confirmed surface area.

NaYF-GO electrodes were fabricated into coin cells for testing in a Lithium Ion Battery system. The enhancement of NaYF's electrochemical activity was confirmed with a total differential capacity versus voltage plot.

1.0 Introduction, Background, Motivation

1.1 The Need for Better Batteries

With the shift away from fossil fuels within the Energy sector, batteries have become an integral part of the plan to reduce greenhouse gas emissions. As a result, more and more industries are looking to expand and utilize electric power, with the automobile industry being a prominent example. Research and development of battery technologies has thus far kept pace with these trends, with Lithium Ion Batteries (LIB) evolving their energy density from 250 to 300 Wh/kg and 600 to 700 Wh/L for the electric vehicle. However, energy demands are increasing with the aviation industry possibly also looking to expand to the electric sector. Higher energy densities, closer to 800-1000+ Wh/kg and around 500 Wh/kg, would be required for LIBs to keep up. LIBs have the advantage over other rechargeable batteries in terms of higher volumetric and gravimetric energy densities. Using non-aqueous electrolytes results in a higher operating voltage for LIBs, approximately 4.0 V, compared to other battery systems using aqueous electrolytes, these systems have a significantly lower operating voltage of around 2.0 V. They have a great range of functions in which they can be used in smaller portable devices to bigger devices such as the electrical vehicle [1-4].

1.2 Why LIBs are not the Sustainable Choice

While LIBs possess a great number of advantages over other battery systems, they do have their disadvantages. The most important of which is the low abundance of elemental Lithium as well as the geometric constraints of its mines. In addition, commonly used electrode materials, such as Cobalt for the cathode, are also rare in abundance. It is predicted that the demand for Lithium for energy storage will far exceed the availability of the metal in the coming years. This is also expected to have a significant impact on the price of these metals. It must also be noted

that the electrode chemistry and battery architecture plays a role in determining the battery energy density. This is also true for LIBs where the energy density is determined by the number of crystallographic sites available and chemical stability of the materials. Research is ongoing to test several other materials and their compatibility with Lithium in batteries, such as Lithium-Sulfur and Lithium-Metal Fluoride battery systems, as well as Lithium free battery systems, such as magnesium ion batteries and sodium ion batteries. This paper will explore a different battery system instead, the Fluoride Ion Battery [1-5].

1.3 Fluoride Ion Batteries: An Alternative

A possible alternative to the LIB system that has gained attention recently is the Fluoride Ion battery (FIB) system. Although the principal charge carrier in this case would be the negatively charged Fluoride anion (F^-) as opposed to the positive Lithium cation (Li^+), FIBs and LIBs still share similar fundamental properties. Higher voltage redox pairs are possible in both LIBs and FIBs, due to the high reduction potential of the Lithium ions and the oxidative potential of the Fluoride ions, with electronegativities of 0.98 and 4.0 respectively. In addition, both Lithium and Fluoride are the smallest and therefore lightest particles within their respective groups and so that allows for higher energy densities and faster ionic transport compared to the other elements of their groups [4-7,13].

In terms of abundance, Fluorine is the 13th most abundant element on earth, existing as Fluorspar (CaF_2) primarily. A major advantage to the FIB argument would be the existence of a long established supply chain, with Fluorspar production spanning four continents and a global production of over 3.5 million tons annually–almost two orders of magnitude higher than that of Lithium. It must be noted that Fluoride can not act as an electrode on its own due to its corrosive nature and gaseous state, it must be deployed with another metal with fluorides acting as the

active material to shuttle the Fluoride anion. In addition, bivalent or trivalent metal Fluorides possess can store a higher number of F^- ions per metal which leads to a higher specific capacity compared to the monovalent metal. Moreover, FIBs offer advantages over LIBs as a result of their multiple-electron redox reactions, such as a theoretical higher volumetric and gravimetric energy densities, and high cell voltage and capacity. There is a lower safety risk associated with FIBs compared to LIBs due to the lack of dendrite growth and exothermic oxygen decomposition [8-13].

FIBs hold immense potential as an electrochemical system. However, there is still much work to be done in the field of FIBs in terms of electrolyte (both solid and liquid), electrode and cell design development and overall optimization. On the other hand, LIBs have the advantage of a well established and studied system therefore they can aid in the development of new electrode materials and other electrochemical testing that can then be applied to FIBs. To that end, this study will utilize LIBs to test the electrode material [15].

1.4 Sodium Yttrium Fluoride (NaYF) Materials for FIBs

Sodium Yttrium Fluoride (NaYF) gel is utilized as the Fluoride metal in this study due to its noteworthy chemistry and relatively large surface area. NaYF materials possess variable stoichiometries based on the levels of combination of Sodium Fluoride (NaF) and Yttrium (III) Fluoride (YF_3) during the gelation reaction. The final stoichiometry of a NaYF material has the form $Na_{0.5-x}Y_{0.5+x}F_{2+2x}$ and has a cubic structure. $NaYF_4$ refers to the final form of the material, attributing to when x approaches zero in the stoichiometry. However, as this study does not assume to be dealing with a perfect cubic structure of the material, the gel will be referred to with the notation NaYF throughout. [15-16]

In their paper [16], Bard et al. investigated the kinetics of crystallization of NaYF gel materials and systems. The paper concluded the NaYF gel crystallization is both chemically driven and multistep. NaYF gel is synthesized through a sol-gel process where two precursor aqueous solutions are mixed at certain concentrations at ambient room temperature and pressure, the process is further described in section 2.1.1 below. The paper concluded the crystallization occurs over four stages: first the aqueous ions separate into a dense liquid phase, then a metastable amorphous aggregate phase forms in a porous gel-like structure, this is followed by the Sodium and Fluoride ions' continual and gradually solid-state diffusion in the amorphous aggregate phase, from a Sodium-poor phase to a Sodium-rich phase, towards the cubic $NaYF_4$ stoichiometry. Finally the amorphous aggregate shifts into the stable cubic phase of $NaYF_4$ and crystallization is complete. The main feature that elevates NaYF as a promising material for electrochemical application is the high surface area of the gel as well as the ion diffusion step following the amorphous aggregate formation. As mentioned above, one of the main constraints of LIB systems is the availability of crystallographic reaction sites on the electrodes. Incorporating NaYF into the electrode will present the unique opportunity to tune and optimize the number of active sites for the electrochemical reaction to occur within the battery, thereby directly affecting its energy density.

In order to investigate the ion solid-state diffusion and the gradual stoichiometric shifting crystallization, an ion replacement experiment was conducted by Bard et al. in [15] and illustrated in **Figure 1** This was done by synthesizing the gel and allowing the diffusion to occur for a certain period of time followed by the isolation and rinsing of the gel in nanopure water and suspending it in another ion solution, in this case Potassium Fluoride (KF), and allowing the crystallization to proceed overnight. The results showed that the amount of sodium ions within the material increased linearly with a corresponding linear decrease of the amount of potassium ions within the material. This experiment highlights the tunability of NaYF gel materials not only

in terms of variable stoichiometry but also opens the gates of discussion for defect engineering of the gel. The spin-lattice relaxation time constant, T_1 ,of the gel was studied and the results showed a higher concentration of Sodium ion defect sites in the amorphous phase compared to the $NaYF_4$ crystalline phase. This, along with the gel's porous surface area, makes NaYF materials attractive candidates for electrochemical applications.

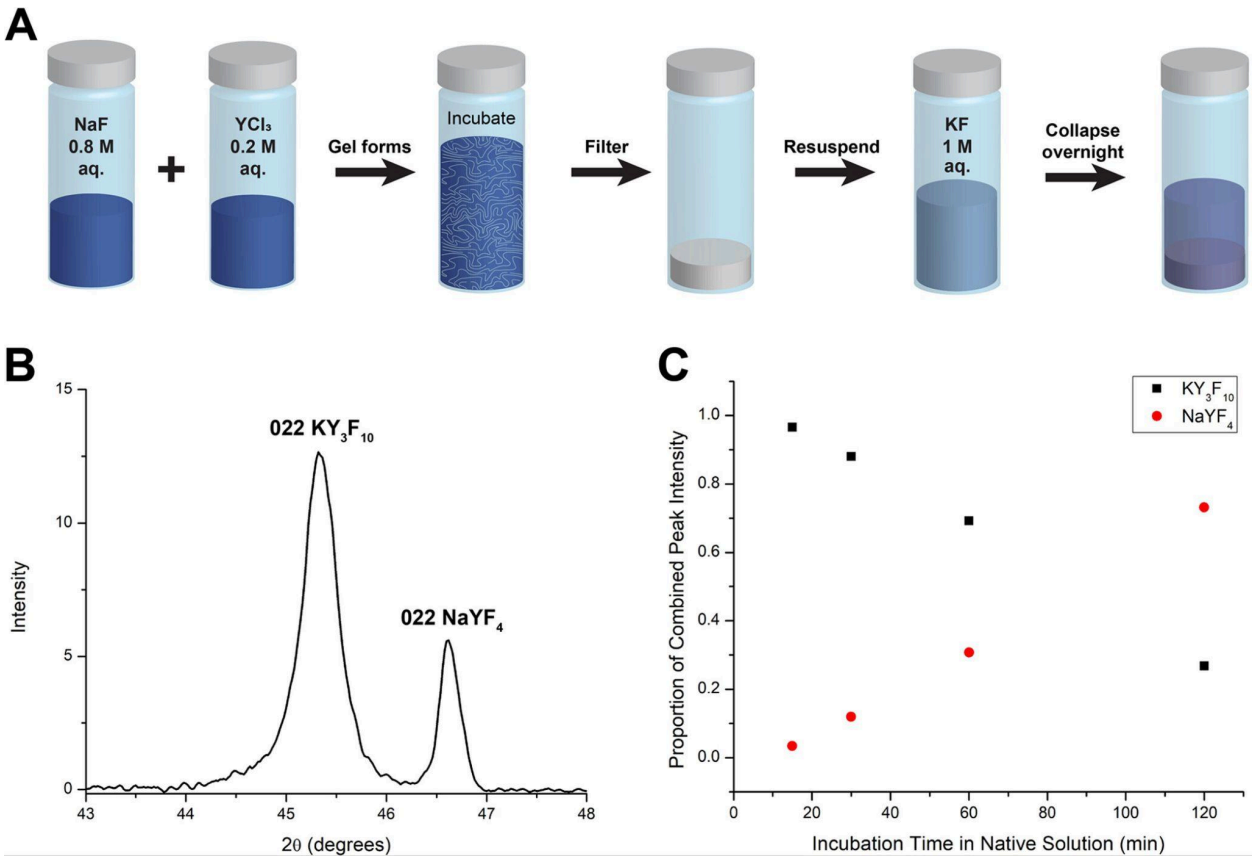

Figure 1 *(adapted from [16]) showing the Ion Replacement Experiment.*

In fact, the reversible cycling of this material has already been demonstrated as an anode for sodium lithium batteries by Bard et al. in the same study [16]. **Figure 2** below shows the cycling data of the NaYF gel as a negative electrode for Li-ion batteries. The total differential capacity versus voltage curves of a battery are used to study and identify changes in electrochemical systems. The differential capacity plots of a battery system serve as a "fingerprint" that is unique

to that specific battery system. These curves provide useful information regarding the thermodynamics and kinetics of the system. The peaks present represent the reactions occurring during the discharge and charge of the battery, lithiation and delithiation, respectively, with the widths of the peaks representing the extent of the reactions. Such plots are important diagnostic tools as the battery's health and changes in the internal electrochemical environment can be deduced from the shifts in the peaks of the curves. We notice the peaks in **Figure 2** are low in intensity and sparse within the curves [16-21].

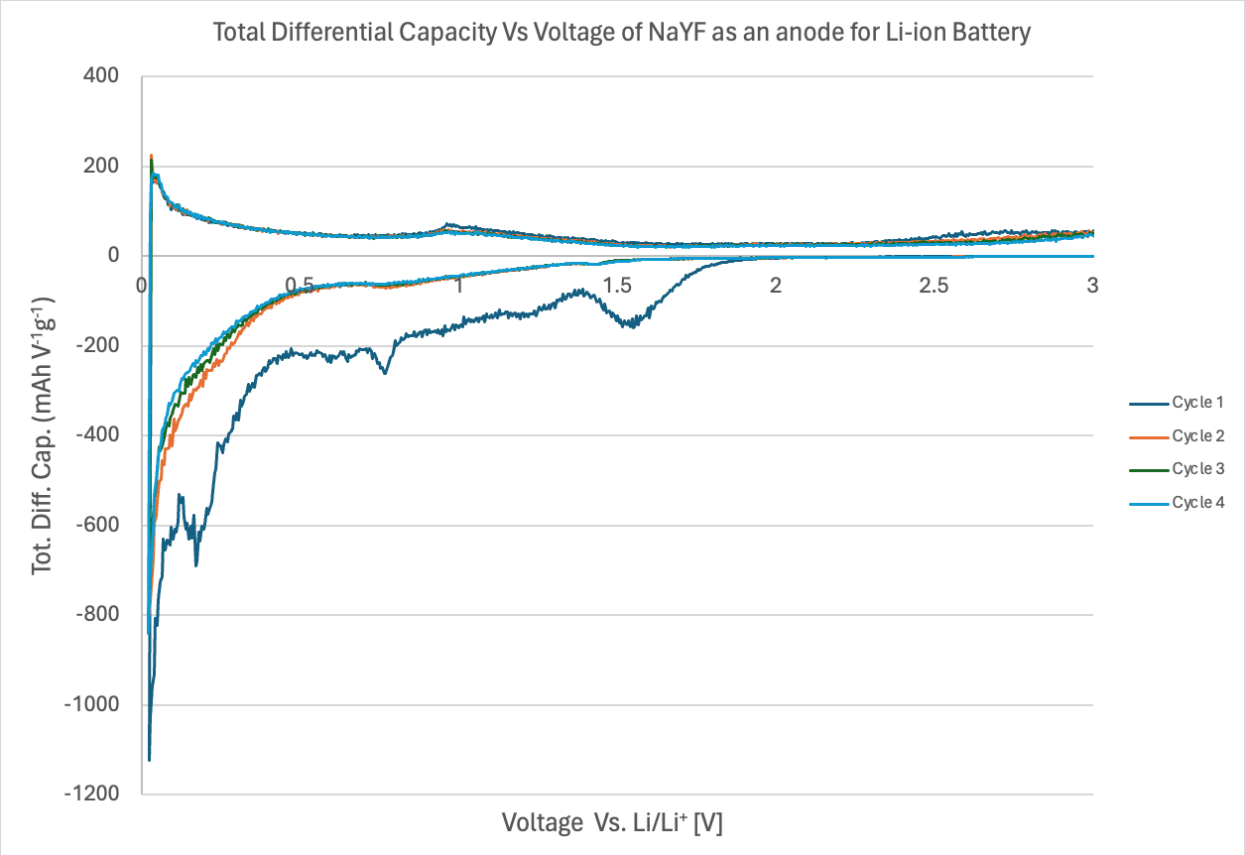

Figure 2 *The cycling data of the NaYF gel as a negative electrode for Li-ion batteries.*

1.5 Integration of Graphene Oxide (GO)

Graphene refers to the two-dimensional (2D) form of sp^2-bonded carbon atoms arranged in a distinct honeycomb lattice structure. Graphene is characterized by remarkable physicochemical properties which include significant mechanical strength, high specific area and thermal conductivity, optical transmittance as well as electron transport properties. When Graphene bonds with functional groups involving oxygen, such as hydroxy, epoxy and carboxyl groups, it is referred to as Graphene Oxide (GO). GO may also be considered a monolayer of Graphite Oxide. Due to its enhanced properties as a result of the oxygenated functional groups, GO has gained significant attention in the scientific community, particularly towards electrochemical application research. The functional groups serve as active sites to immobilize electroactive species which allows the opportunity for further functionalization and chemical modification of GO within a battery system. As GO is uniquely considered an amphiphilic material due to the hydrophilic carboxyl groups and the hydrophobic polyaromatic network of carbon rings, it can be incorporated in various electrochemical energy systems from batteries to capacitors and fuel cells for a multitude of different system conditions through self-assembly. GO can be introduced to electrochemical systems in aqueous dispersions to pair with another phase. This allows for GO to be incorporated into these systems with specifically tuned properties and controlled microstructures. Research and previous studies have already investigated the effect of the Graphene Oxide inclusion to specific battery systems, capacitors, and fuel cells, particularly its role in LIBs and Sodium Ion Batteries (SIB). Due to its oxygenated functional groups, Graphene Oxide has been used in both electrodes and electrolytes as well as integrated as fillers or protective membranes in certain systems [22-23].

1.6 Motivation/thesis statement

The motivation of this study is to investigate and characterize the incorporation of Graphene Oxide into a Sodium Yttrium Fluoride gel for electrochemical applications eventually for Fluoride ion batteries. The study will test the hypothesis that the conductivity of NaYF as an electrode will be enhanced and the overall battery performance will improve with the addition of Graphene Oxide. To this end, the NaYF-GO gel was synthesized, underwent supercritical drying and then fabricated into a coin cell in a Lithium Ion Battery system and cycled at a current of 0.1mA, corresponding with a current density of 143 mA g^{-1}, at cycling rates of 1C, C/10, and C/20.

2.0 Methodology

2.1.1 NaYF-GO Gel Synthesis

The sol-gel synthesis of NaYF used in this study was adapted from [16] and modified to include GO. The synthesis utilized Sodium Fluoride (NaF), Yttrium (III) Chloride Hexahydrate and Graphene Oxide (Multilayer, 15-20 sheets, 4-10% edge oxidized) from Sigma Aldrich as reagents. Precursor aqueous solutions of NaF in a 0.8 M concentration and YCl_3 in 0.2 M concentration were prepared. 10 mg/ml of Graphene Oxide was introduced to the system through the addition to either of the precursor solutions followed by a vortexing step. It should be noted that iterations of the experiment proved the gel formation occurred regardless of which of the precursor solutions the Graphene Oxide was introduced to initially. The gel forms once the solutions are mixed together at ambient room temperature and pressure. This step is followed by a centrifugation at 4000 RPM for 1 minute in order to crash out the gel. It then undergoes a washing step, with water initially and then with ethanol, for a solvent exchange process to prepare the gel for the drying process. This is carried out through the decantation of the solvent (water) and replacing it with another solvent, water again once and then twice with ethanol with another centrifugation step in between each solvent, once more at 4000 RPM for 1 minute, respectively. It is vital for a vortexing step to exist between the switch from water to ethanol to ensure the solvent can penetrate the gel completely for the solvent exchange process, otherwise the crystallization of the NaYF gel will continue to occur due to existence of water still in the pores of the gel.

2.1.2 Drying the NaYF-GO Gel

In [16], the NaYF gel was collected in a Buchner funnel under vacuum, rinsed with water and ethanol and then allowed to dry, resulting in a xerogel. In this study, however, the gel was dried using two different methods: supercritical drying, producing an aerogel, and freeze drying, or lyophilization, which produced a cryogel. Although all of these methods result in the removal of the solvent from the gel, the varying methodologies associated with each result in variations in pore size and structural properties of the gel. Supercritical drying is a process where the solvent within the gel, ethanol, is replaced with a supercritical solvent, in this case it is Carbon Dioxide (CO_2) in a pressurized vessel at supercritical conditions, 31.3℃ and 72.9 bar, allowing for the system to dry without passing through the liquid–gas phase boundary. This process is most favored for the drying of gels as it preserves the porous structure best due to the lower surface tension of the supercritical fluids [24-25].

Freeze drying produces cryogels through the freezing of the solvent within the gel followed by its sublimation, leaving behind the nanostructure of the gel intact [19]. Although the NaYF-GO gel was proved to be compatible with both the freeze drying and supercritical drying processes, the scope of this study will be limited to the characterization and electrochemical performance of the supercritical dried NaYF-GO gel [24-25].

2.1.3 NaYF-GO Gel Characterization

The gel underwent several characterization testing including X-Ray Diffraction Analysis (XRD) to determine the crystalline structure. This technique relies on passing an X-ray beam, the incident beam, through the sample and analyzing the resulting variance in angle, theta, from the angle of the original beam, as the X-rays “bounce off” structures within the crystal–this is referred to as the angle of diffraction. Bragg’s Law, which relates the angle of diffraction, theta (θ), to the

wavelength (λ) through equation (1) below, can then be used to determine the sample's crystal structure.

$$Sin(2\theta) = \frac{n\lambda}{2d} \qquad \textit{(Equation 1)}$$

X-rays are utilized in this technique as their wavelength is of similar magnitude to the spacing between atoms and would therefore have an effect on the angle of diffraction. The final result of an XRD analysis is a plot of intensity versus 2θ, the angle of diffraction. The 2theta positions on the plot correspond to certain crystalline spacings within the sample. The intensity of the peak is linearly related to the relative amounts of that distinct spacing within the sample while the width of the peak is inversely related to the crystal size. A sharp peak alludes to a large or highly crystalline structure while a broad peak suggests the existence of crystal defects or an amorphous nature of the sample [26].

To further investigate the atomic structure in terms of crystallinity and to further confirm the uniform integration of Graphene Oxide into the gel, Transmission Electron Microscopy (TEM) and Tomography tests were conducted. TEM aims an electron beam on an extremely thin sample which then either diffracts the beam or simply lets it pass through. The interactions of the resulting diffracted image and the magnified image within the microscope can then be analyzed to reveal information about the sample structure in the nanoscale. Tomography is a technique based on the mathematical concept of Radon transformations where a 3D rendering of an object or material is created through a series of 2D images tilted at slightly different angles. Tomography is significantly important in material science as the 3D rendering of a sample can give ample information about the structure of a material, especially in cases such as ours where we have a porous gel structure [27-28].

In addition, Brunauer-Emmett-Teller theory (BET) analysis was employed to determine the surface area of the porous NaYF-GO gel. BET theory is an extension of the Langmuir theory, which relates the monolayer gas adsorption on a solid surface to the gas pressure at a fixed temperature, to a multilayer adsorption. Nitrogen gas is usually utilized for BET due to its strong interaction with most solids as well as availability. The sample is degassed, cooled using liquid nitrogen, and then injected with known amounts of gas. The adsorption and desorption data is then collected and plotted. Typical BET analysis results are in the form of an isotherm plot relating the amount of gas adsorbed as a function of relative pressure of the system. The surface area can then be determined from the isotherm as well as the BET equation. Some instruments, such as the one used in this study, will calculate that automatically using the equipment software [29].

It is noteworthy to mention that all characterization has been carried out on the supercritical dried NaYF-GO sample and prior to the electrochemical testing of the gel.

2.1.4 Coin Cell Fabrication

Following the characterization testing, the supercritical dried gel was then used to fabricate coin cell electrodes in order to test their electrochemical performance. NaYF-GO was to act as the negative electrode, the anode, in this configuration due to its electronegativity, with elemental Lithium metal acting as the cathode, the positive electrode, and 1.0 M Lithium Hexafluorophosphate ($LiPF_6$) in EC/DMC. NaYF-GO was loaded onto a Copper current collector.

The electrodes were prepared in a 70:20:10 NaYF-GO:Conductive Carbon:Binder ratio. In this study the binder used was Polyacrylic acid (PAA) in N-Methylpyrrolidone (NMP) with a density of 51.4 mg/mL. Accordingly, 80 mg of NaYF-GO gel were combined with 11 mg of Conductive Carbon and 0.108 µL of the binder were combined and mixed into a slurry in a mortar and pestle. The slurry was then spread and doctor bladed on a Copper film with a 5 µm thickness in a fume hood. The electrodes were allowed to dry first on a hot plate (80℃) in air and then further in a vacuum oven (90℃) overnight. 15 mm punch outs were created from the Copper strips and the weight of the electrode was averaged around 8.49 g with about 0.69 active material. The coin cells were fabricated in an Argon glove box. The cell was assembled in the following parts, bottom up: Stainless steel cup, electrode on copper current collector (anode), glass fiber separator, plastic spacer, electrolyte, lithium foil, stainless steel spacer, stainless steel wave washer, and finally the stainless steel cap. The coin cells were finally crimped into shape and were then ready for testing. Coin cell testing was carried out by the MACOOR Series 4000M 64-Channel Automated battery test system using a current of 0.1mA corresponding with a current density of 143 mA g^{-1}. The coin cells cycled at rates of 1C, C/10, and C/20.

2.1 Results and discussion

2.2.1 Synthesis and drying results

Almost immediately upon the mixing of the precursor solutions at their relative concentrations in atmospheric conditions, the gel-like structure materialized within the tube. After centrifugation and the solvent exchange process, the gel appeared as a dark gray solid, as opposed to the translucent solid NaYF gel reported in [16]. This can be traced to the addition of the GO in the synthesis. **Figure 3** below shows the gel (a) after the solvent exchange process and (b) after the supercritical drying process. The supercritical dried NaYF-GO gel had a lighter gray

appearance compared to the wet gel. In addition, as the gel contained both a degree of amorphousness and GO, it was light and susceptible to holding static.

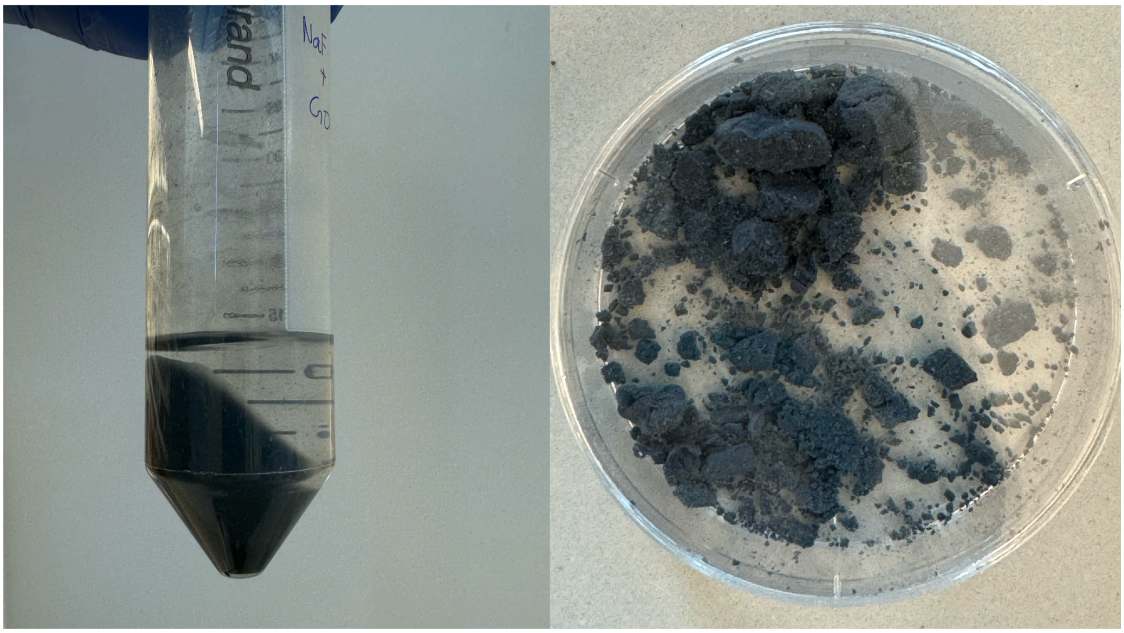

Figure 3 *NaYF-GO in (a) gel form and (b) after supercritical drying.*

2.2.2 XRD

XRD testing was conducted on the supercritical dried NaYF-GO sample, the results can be seen in **Figure 4**. The results show an amorphous material, evident by the larger humps roughly between 25 and 35 degrees as well as those between 40 and 50 degrees, with some crystallinity, evident by the sharper peaks around 40 degrees as well as 57 degrees, as expected. A materials search was conducted on the scan to identify the expected crystal structures: α-NaYF, possibly β- NaYF, NaCl, NaF as well as any Carbon product resulting from GO's presence. **Figure 4** below highlights the peaks detected. We notice the sharpest peaks correlate to NaF and α-NaYF which was expected as these are highly structured crystals. While NaF, NaCl were present, they had peaks with low intensity and were most likely associated with unreacted elements, the case of NaF, or byproducts of the reaction, in the case of NaCl. β-

NaYF also had peaks with low intensity which was expected as this synthesis method favors the formation of α-NaYF over β- NaYF. Finally, the XRD results confirm the presence of Graphene Oxide in the form of Graphite, though the peaks also show low intensity.

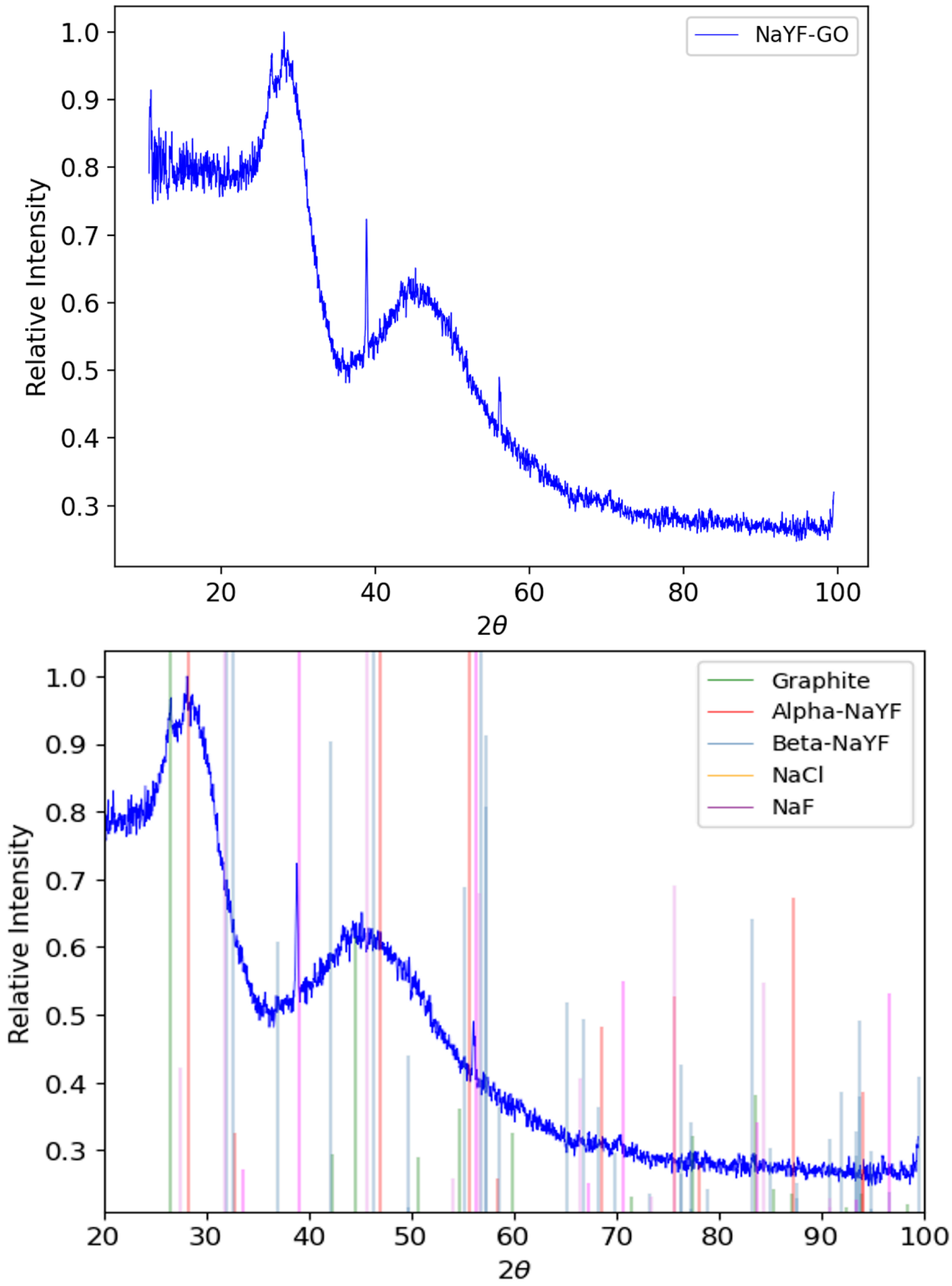

Figure 4 *XRD of the NaYF-GO gel with and without peak identification.*

2.2.3 TEM

TEM and tomography imaging tests were performed in order to observe the NaYF-GO structure and cohesiveness. **Figure 5** below shows TEM images of the gel at 0.2 μm, 0.5 μm, 200 nm, 50 nm, and 10 nm. At 0.2 μm and 0.5 μm we observe the general structure of the gel and notice a darker cloud concentrated in certain areas of the gel, which is assumed to be Graphene Oxide. The nonuniformity in appearance here can either mean that the GO is not fully combined within the gel or may suggest that the amount of GO used in the synthesis requires adjustment. At 0.2 μm we can also observe what could be a graphene sheet, marked on the figure below. It can also be observed in the tomography video of the sample. At 200 nm, the porous structure is clearly visible and is comparable with the TEM images presented in [16]. The darker spots within the pores of the gel can be assumed to be GO. The TEM image at 50 nm proves our earlier assumption that GO will sit within the pores of the NaYF gel. This can be clearly seen in the Figure, where it is outlined with a purple circle, we notice sheets of GO perfectly aligned on its side within the pores of the gel. At 10 nm, the crystalline structure of the material is apparent. However, it can be noticed that the crystalline structure is not completely uniform, we recall from the XRD results that the gel contains a certain degree of crystallinity but is mostly amorphous.

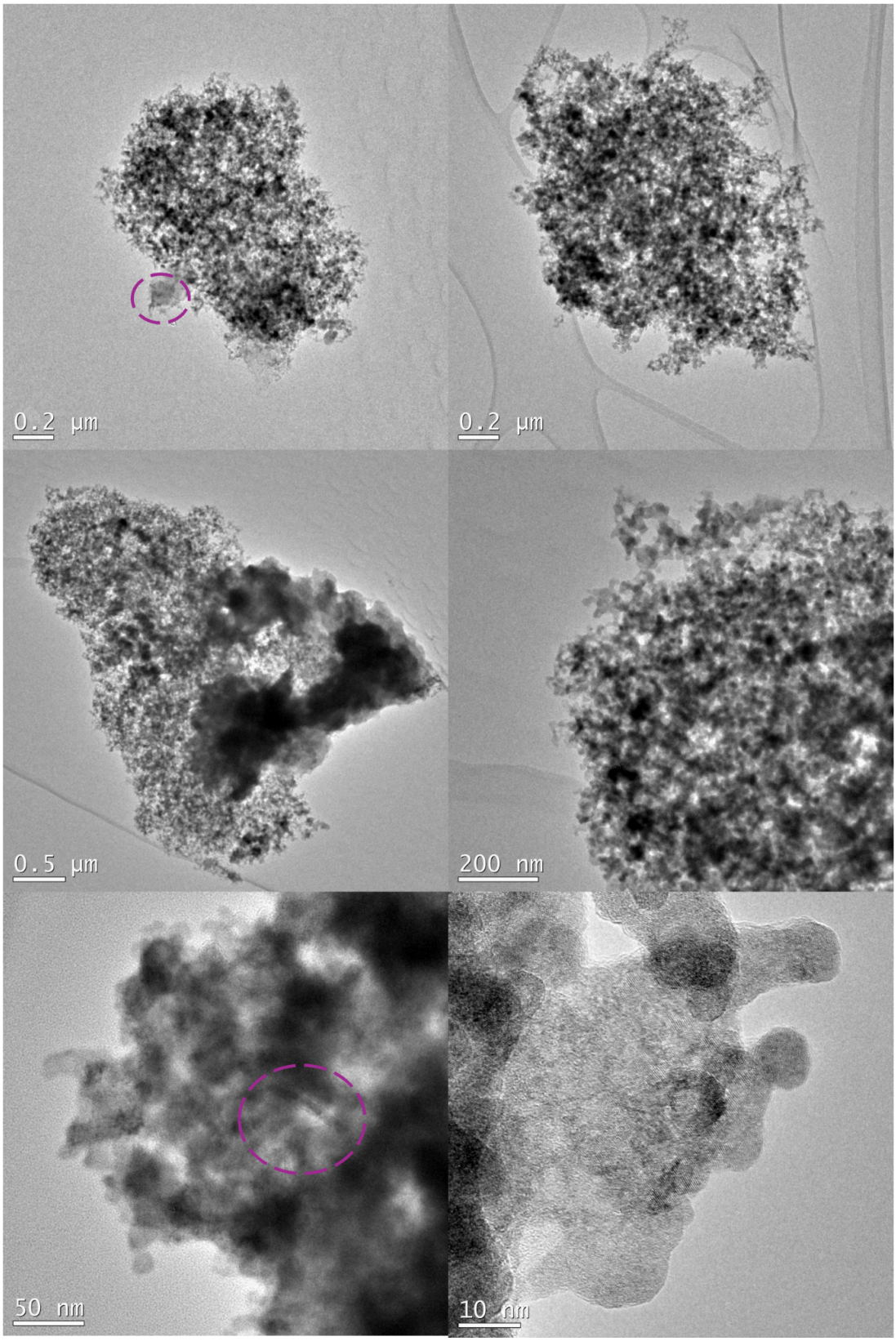

Figure 5 *TEM imaging of the NaYF-GO gel at 0.2 µm, 0.5 µm, 200 nm, 50 nm, and 10 nm.*

2.2.4 BET

BET Analysis was carried out for the gel at both 150 ℃ and 250 ℃ and the resulting surface area was 111.004 m^2/g and 88 m^2/g, respectively. This is consistent to what Bard et al. reported in [16] where the surface area was measured to be 100 m^2/g. The slightly higher results can be linked to the difference in drying methodology of the gel as aerogels tend to have larger surface areas compared to xerogels due to the tension and stress factors within the pores during the drying process [23-24].

2.2.5 Electrochemical Characterization

Figure 6 below illustrates the total differential capacity versus voltage plot of the LIB system with the NaYF-GO electrode. Instantly we can recognize that ,compared to **Figure 2**, the GO introduction to the NaYF altered and enhanced the electrode's electrochemical expression, as evident by the strong peaks present. As stated earlier, these peaks are proof of the electrochemical reactions occurring within the battery. These results confirm the electrochemical activity increased within the NaYF electrode with the incorporation of Graphene Oxide [21].

These results highlight the flexibility of the NaYF system for electrochemical applications in particular. We recall the ion replacement experiment conducted with NaYF in [16] and how substituting the incubating solvent from water to Potassium Fluoride (KF) resulted in the introduction of K^+ ions within the NaYF matrix and the formation of KY_3F_{10}. We also recall the energy density is determined, in part, by the number of crystallographic sites available in the system. The two factors underpin NaYF's incredible potential in electrochemical systems with its high surface area and affinity for ion exchange which can lead to intentional defect engineering to further enhance the gel as an electrode material.

There may be the argument that these peaks in the total differential capacity plot are a result of the Graphite present in the sample, as confirmed by the XRD data earlier. However, there are evident peak shifts and differences within similar cycling rates when comparing **Figure 6** and **Figure 7**, which shows the total differential capacity versus voltage of a Graphite electrode and that of a NaYF-GO electrode in a LIB system at a cycling rate of 1C. For the Graphite electrode, the first peak was around 0.2016 V and the second peak around 0.2831 V. Whereas for the NaYF-GO electrode, the first peak was 0.962 V and the second around 0.142 V. The minimal shifts in peaks within the NaYF-GO system alludes to a more efficient electrochemical system as there is a lower energy loss as heat associated with the change in voltage when compared to the shifts in Graphite peaks. This may also be explained by the nanoscale phenomena as NaYF-GO is in the nanoscale while Graphite is not. The nanoscale phenomena refers to the alterations of properties materials go through when shifted from the micro to the nanoscale. This includes changes in kinetics, thermodynamics as well as augmentation of surface area which is an important aspect to consider in electrochemical processes and applications [30].

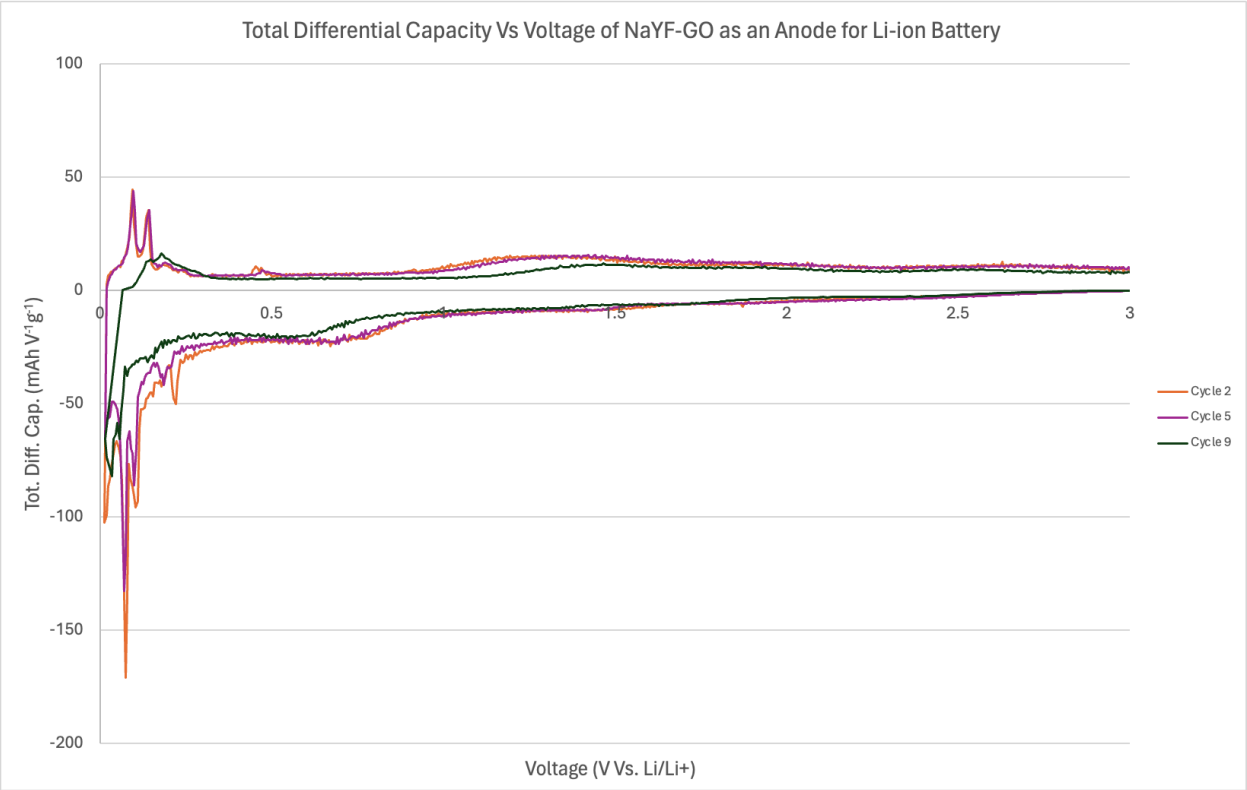

Figure 6 *Total Differential Capacity Versus Voltage of NaYF-GO as an Anode for Li-Ion Battery System.*

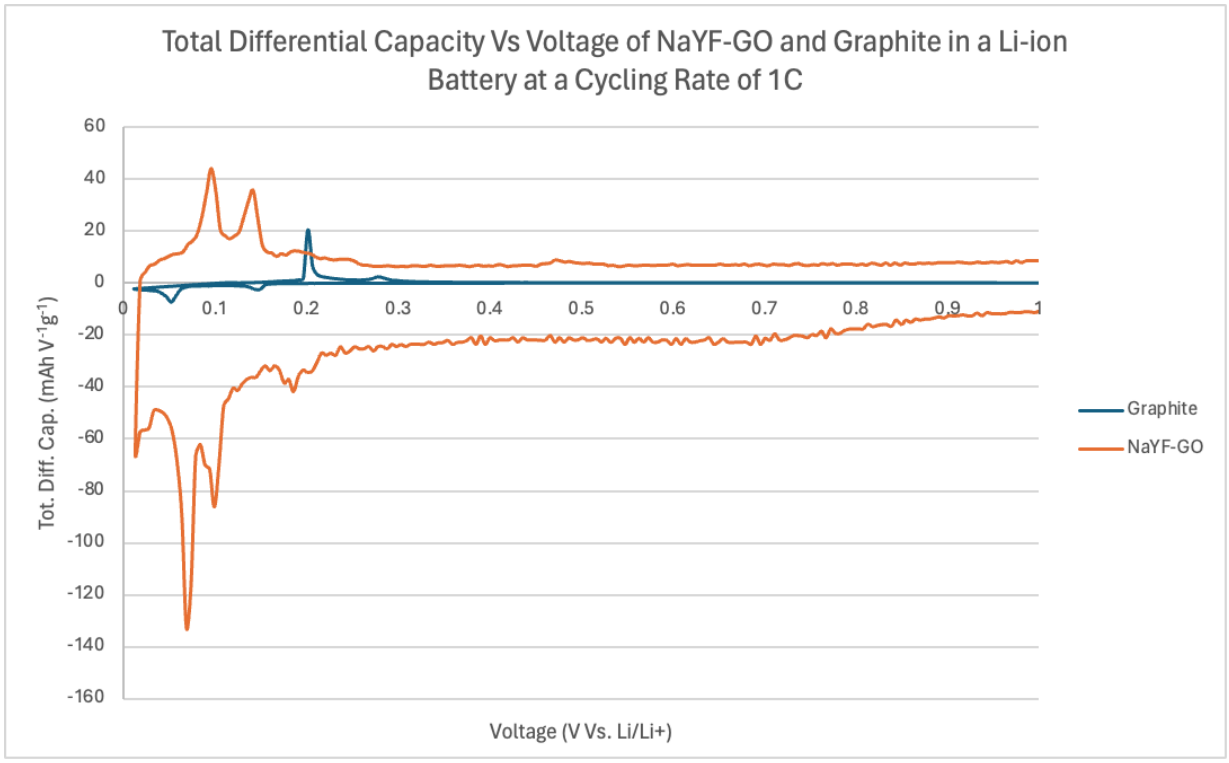

Figure 7 *Total Differential Capacity Versus Voltage of Graphite and NaYF-GO a in Li-ion Battery at a Cycling Rate of 1C.*

3.0 Conclusions and Future works

3.1 Conclusion

In order to cope with the ongoing climate crisis as well as the rising demands in energy, batteries research must continue to develop batteries with higher energy densities. Lithium ion batteries are well established and studied electrochemical systems but face disadvantages in abundance of materials, Lithium and Cobalt for the cathodes, as well as higher costs. Fluoride ion batteries offer an alternative that's more abundant in raw materials and less expensive. However, it also requires further research to optimize the battery system in terms of its electrolyte, electrodes as well as its battery cell architecture. To that end, the NaYF-GO gel was tested in a LIB system. The multistep crystallization in NaYF gel systems along with its high surface areas as well as the affinity for ion replacement position the material as a great candidate for electrochemical applications. Graphene Oxide was integrated to upgrade the NaYF gel's conductivity as an electrode material.

This study confirmed that Graphene Oxide can be integrated into the Sodium Yttrium Fluoride gel through the simple addition to the precursor solutions. The NaYF-GO gel proved to be compatible with both freeze drying and supercritical drying methods. The dried gel was a dark gray, attributed to the presence of GO. The gel's static and light nature was explained through XRD where it was confirmed that the gel is mostly amorphous, hence the light and static nature, with some degree of crystallinity. Furthermore, XRD confirmed Graphene Oxide's presence through the existence of low intensity Graphite peaks. TEM imaging further confirmed the porous structure of the gel as well as the integration of the Graphene Oxide within the gel's pores. BET analysis performed at 150 °C and 250 °C and resulted in surface areas of 111.004 m^2/g and 88 m^2/g, respectively. This is consistent to what Bard et al. reported in [16] where the

surface area was measured to be 100 m^2/g. Finally, the addition of Graphene Oxide to NaYF gel proved to enhance its electrochemical performance as a electrode for Lithium Ion batteries, as evident by the emergence of sharp peaks in the total differential capacity versus voltage plots and compared to those plots of NaYF electrodes in the same system. The existence of Graphite in the gel, as confirmed through XRD, can not take full credit for the electrochemical enhancement of the NaYF electrodes as the total differential capacity versus voltage plots of Graphite batteries observe different peaks and peak shifts with varying cycling rates compared to that of NaYF-GO. In addition, NaYF-GO electrodes showed a smaller energy loss compared to Graphite electrodes with the transitions of cycling rates, suggesting that the NaYF-GO electrode was more efficient.

3.2 Future works

The most intriguing aspect of research is its Hydra-like nature, we can answer one question and seven more will sprout in its place, this project was not the exception to that. While we did prove Graphene Oxide's integration into the NaYF gel as well as its effect on the electrochemical performance of LIB systems, these results open up the possibility for further research in multiple areas.

The main question would be: now that we know it works, how can we make it better, i. e how to best optimize the system. In terms of synthesis, the multistep crystallization nature of the NaYF gel adds a layer of complexity and flexibility to the system. As illustrated by Bard et. al in [15] through the ion replacement experiment, the incubation time of the gel as well as the solution it is incubated within both have a profound effect on the gel's composition, crystallinity and amount of defects and therefore on its properties. The amount of Graphene Oxide introduced to the system may also be altered and its effect should be studied in terms of both its integration

within the gel as well as its electrochemical performance. The number of Graphene Oxide sheets can also be varied as this study employed multilayer (15-20 sheets). An interesting area of research may be the effect of the GO sheet orientations within the pores on its electrochemical performance. This may be explored through electrical field manipulation of the Graphene Oxide sheets within the gel, as presented in [31]. Furthermore, this study only examined the supercritical dried NaYF-GO gel. As different drying methods produce gels with different properties and pore size, it may also be worthwhile to perform a similar optimization and electrochemical analysis on a gel that's been freeze dried.

In terms of electrochemical analysis, coin cells may be fabricated with different compositional ratios other than the 70:20:10 presented in this paper. Moreover, varying the electrolyte used may affect the battery performance and is worth exploring. Of course, as this paper explored the effects of GO integration into NaYF gel on its electrochemical performance in a LIB system, the end goal is for further testing in a FIB system.

Bibliography

[1] A. Manthiram, “An Outlook on Lithium Ion Battery Technology,” *ACS Central Science*, vol. 3, no. 10, pp. 1063–1069, Sep. 2017, doi: https://doi.org/10.1021/acscentsci.7b00288.

[2] A. W. Schäfer *et al.*, “Technological, economic and environmental prospects of all-electric aircraft,” *Nature Energy*, vol. 4, no. 2, pp. 160–166, Dec. 2018, doi: https://doi.org/10.1038/s41560-018-0294-x.

[3] A. El Kharbachi, O. Zavorotynska, M. Latroche, F. Cuevas, V. Yartys, and M. Fichtner, “Exploits, advances and challenges benefiting beyond Li-ion battery technologies,” *Journal of Alloys and Compounds*, vol. 817, p. 153261, Mar. 2020, doi: https://doi.org/10.1016/j.jallcom.2019.153261.

[4] A. W. Xiao, G. Galatolo, and M. Pasta, “The case for fluoride-ion batteries,” Joule, vol. 5, no. 11, pp. 2823–2844, Nov. 2021, doi: https://doi.org/10.1016/j.joule.2021.09.016.

[5] M. Anji Reddy and M. Fichtner, “Batteries based on fluoride shuttle,” *Journal of Materials Chemistry*, vol. 21, no. 43, p. 17059, 2011, doi: https://doi.org/10.1039/c1jm13535j.

[6] X. Hou *et al.*, “An Aqueous Rechargeable Fluoride Ion Battery with Dual Fluoride Electrodes,” *Journal of The Electrochemical Society*, vol. 166, no. 12, pp. A2419–A2424, 2019, doi: https://doi.org/10.1149/2.0301912jes.

[7] V. K. Davis *et al.*, “Room-temperature cycling of metal fluoride electrodes: Liquid electrolytes for high-energy fluoride ion cells,” *Science*, vol. 362, no. 6419, pp. 1144–1148, Dec. 2018, doi: https://doi.org/10.1126/science.aat7070.

[8] W. M. Haynes, *CRC Handbook of Chemistry and Physics, 95th Edition*. Taylor & Francis Ltd, 2014.

[9] M. G. García and L. Borgnino, “CHAPTER 1 Fluoride in the Context of the Environment,” *pubs.rsc.org*, pp. 3–21, 2015, doi: https://doi.org/10.1039/9781782628507-00003.

[10] “Mineral Commodity Summaries,” *Usgs.gov*, 2021. https://www.usgs.gov/centers/nmic/mineral-commodity-summaries

[11] M. Zhou, L. Zhao, T. Doi, S. Okada, and J. Yamaki, “Thermal stability of FeF3 cathode for Li-ion batteries,” *Journal of Power Sources*, vol. 195, no. 15, pp. 4952–4956, Aug. 2010, doi: https://doi.org/10.1016/j.jpowsour.2010.02.076.

[12] M. Zhou, L. Zhao, S. Okada, and J. Yamaki, “Thermal characteristics of a FeF3 cathode via conversion reaction in comparison with LiFePO4,” *Journal of power sources*, vol. 196, no. 19, pp. 8110–8115, Oct. 2011, doi: https://doi.org/10.1016/j.jpowsour.2011.05.042.

[13] G. Karkera, M. A. Reddy, and M. Fichtner, “Recent developments and future perspectives of anionic batteries,” *Journal of Power Sources*, vol. 481, p. 228877, Jan. 2021, doi: https://doi.org/10.1016/j.jpowsour.2020.228877.

[14] Fedorov, P. P. Systems of Alkali and Rare-Earth Metal Fluorides. Russ. J. Inorg. Chem. 1999, 44, 1792−1818.

[15] Mohammad Ali Nowroozi, I. Mohammad, Palanivel Molaiyan, K. Wissel, M. Anji Reddy, and O. Clemens, “Fluoride ion batteries – past, present, and future,” *Journal of materials chemistry. A, Materials for energy and sustainability*, vol. 9, no. 10, pp. 5980–6012, Jan. 2021, doi: https://doi.org/10.1039/d0ta11656d.

[16] A. B. Bard *et al.*, “Chemically Driven Multistep Crystallization in the Synthesis of Sodium Yttrium Fluoride Via a Porous, Electrochemically Active Intermediate,” *Journal of physical chemistry. C./Journal of physical chemistry. C*, Jul. 2024, doi: https://doi.org/10.1021/acs.jpcc.4c01281.

[17] X. Hua *et al.*, “Revisiting metal fluorides as lithium-ion battery cathodes,” *Nature Materials*, vol. 20, no. 6, pp. 841–850, Jan. 2021, doi: https://doi.org/10.1038/s41563-020-00893-1.

[18] M. Kazazi, P. Abdollahi, and M. Mirzaei-Moghadam, “High surface area TiO2 nanospheres as a high-rate anode material for aqueous aluminium-ion batteries,” *Solid State Ionics*, vol. 300, pp. 32–37, Feb. 2017, doi: https://doi.org/10.1016/j.ssi.2016.11.028.

[19] H. Zhang *et al.*, “High specific surface area porous graphene grids carbon as anode materials for sodium ion batteries,” *Journal of Energy Chemistry*, vol. 31, pp. 159–166, Apr. 2019, doi: https://doi.org/10.1016/j.jechem.2018.06.002.

[20] X. Ma, J. Xia, X. Wu, Z. Pan, and P. K. Shen, “Remarkable enhancement in the electrochemical activity of maricite NaFePO4 on high-surface-area carbon cloth for sodium-ion batteries,” *Carbon*, vol. 146, pp. 78–87, May 2019, doi: https://doi.org/10.1016/j.carbon.2019.02.004.

[21] Energsoft - Predictive Battery Analytics Software, “Differential capacity analysis,” *Energsoft - Predictive Battery Analytics Software*, 2018. https://energsoft.com/blog/f/differential-capacity-analysis#:~:text=DqDv%20Curve%3A%20Differential%20capacity%20tracks (accessed Jul. 24, 2024).

[22] A. K. Geim, “Graphene: Status and Prospects,” *Science*, vol. 324, no. 5934, pp. 1530–1534, Jun. 2009, doi: https://doi.org/10.1126/science.1158877.

[23] Y. Tian, Z. Yu, L. Cao, X. L. Zhang, C. Sun, and D.-W. Wang, “Graphene oxide: An emerging electromaterial for energy storage and conversion,” *Journal of Energy Chemistry*, vol. 55, pp. 323–344, Apr. 2021, doi: https://doi.org/10.1016/j.jechem.2020.07.006.

[24] D. Bokov et al., “Nanomaterial by Sol-Gel Method: Synthesis and Application,” Advances in Materials Science and Engineering, vol. 2021, pp. 1–21, Dec. 2021, doi: https://doi.org/10.1155/2021/5102014.

[25] A. Lamy-Mendes, R. F. Silva, and L. Durães, “Advances in carbon nanostructure–silica aerogel composites: a review,” Journal of Materials Chemistry A, vol. 6, no. 4, pp. 1340–1369, Jan. 2018, doi: https://doi.org/10.1039/C7TA08959G.

[26] “X-ray diffraction (XRD) basics and application,” Chemistry LibreTexts, Apr. 14, 2019. https://chem.libretexts.org/Courses/Franklin_and_Marshall_College/Introduction_to_Materials_Characterization__CHM_412_Collaborative_Text/Diffraction_Techniques/X-ray_diffraction_(XRD)_basics_and_application

[27] P. Raja and A. Barron, “8.2: Transmission Electron Microscopy,” Chemistry LibreTexts, Jul. 14, 2016. https://chem.libretexts.org/Bookshelves/Analytical_Chemistry/Physical_Methods_in_Chemistry_and_Nano_Science_(Barron)/08%3A_Structure_at_the_Nano_Scale/8.02%3A_Transmission_Electron_Microscopy

[28] P. Ercius, O. Alaidi, M. J. Rames, and G. Ren, “Electron Tomography: A Three-Dimensional Analytic Tool for Hard and Soft Materials Research,” Advanced materials (Deerfield Beach, Fla.), vol. 27, no. 38, pp. 5638–5663, Oct. 2015, doi: https://doi.org/10.1002/adma.201501015.

[29] P. Raja and A. Barron, “2.3: BET Surface Area Analysis of Nanoparticles,” Chemistry LibreTexts, Jul. 13, 2016. https://chem.libretexts.org/Bookshelves/Analytical_Chemistry/Physical_Methods_in_Chemistry_and_Nano_Science_(Barron)/02%3A_Physical_and_Thermal_Analysis/2.03%3A_BET_Surface_Area_Analysis_of_Nanoparticles

[30] S.-K. Jung et al., “Nanoscale Phenomena in Lithium-Ion Batteries,” Chemical Reviews, vol. 120, no. 14, pp. 6684–6737, Dec. 2019, doi: https://doi.org/10.1021/acs.chemrev.9b00405.

[31] M. B. Lim, R. G. Felsted, X. Zhou, B. E. Smith, and P. J. Pauzauskie, “Patterning of graphene oxide with optoelectronic tweezers,” Applied physics letters, vol. 113, no. 3, Jul. 2018, doi: https://doi.org/10.1063/1.5025225.